Near-field optical response of a two-dimensional grating of gold nanoparticles

M. Salerno, N. Félidj, J. R. Krenn, A. Leitner, and F. R. Aussenegg

*Institute for Experimental Physics, Karl-Franzens-University Graz and Erwin Schrödinger Institute for Nansoscale Research,
Universitätsplatz 5, A-8010 Graz, Austria*

J. C. Weeber

Laboratoire de Physique, Optique Submicronique, Université de Bourgogne, Boite Postale 47870, F-21078 Dijon, France

This article reports on the near-field optical response of a small square grating of gold nanoparticles tailored by electron-beam lithography. The investigation of the grating is aimed at a deepened understanding of electromagnetic interaction among particles due to scattered light fields. Therefore, a photon scanning tunneling microscope is applied to acquire near-field optical images. Two different incident wavelengths are used to characterize the intensity and the spatial localization of the electromagnetic near field both in and out of resonance for the excitation of particle plasmons. Furthermore, the near-field enhancement resulting from the plasmon excitation is evaluated.

I. INTRODUCTION

Nanoscale metal structures are well known to manifest strong local enhancement of the electromagnetic field with respect to the incident light, due to the excitation of coherent resonant electron plasma oscillations (particle plasmons).[1] The resonance wavelength of this phenomenon depends on the geometry of the structure as well as on the dielectric functions of both the structure and the surrounding medium.[2] Since metal nanostructures are promising candidates for such nano-optical applications as controlling and guiding light fields on the submicrometer scale,[3–6] they are the subject of extensive fundamental research. In this context, specifically designed nanostructures obtained by electron-beam lithography (EBL) represent ideal samples for a fundamental systematic investigation. EBL is a powerful tool for the fabrication of highly reproducible nanostructures with a great variety of geometries and arrangement patterns.[7] In particular, it allows matching of the particle plasmon frequencies to defined values.

As for many practical applications large ensembles of nanoparticles are of interest,[8] a better understanding of electromagnetic coupling effects among nanoparticles is of great importance. Coupling can arise both from very short distance interactions (on the order of some tens of nanometers, near-field coupling) and from long range interactions (dipolar far-field coupling[9]). Recently, direct observations of the near-field response of an isolated gold nanoparticle and of a one-dimensional (1D) chain of gold nanoparticles by means of near-field optical microscopy were reported.[10] It was shown that the individual particle gives rise to a rather broadly distributed plasmon field, while a strong confinement of the field was observed above the particle chain due to plasmon near-field coupling. On the other hand, electromagnetic far-field coupling was found to be particularly strong among nanoparticles arranged in regular 2D particle gratings.[11] When the interparticle distance is increased for a given light wavelength, dipolar interaction between the particles increases dramatically whenever the light field corresponding to a particular grating order changes from evanescent to radiative in character. As a consequence, a strong dependence of the plasmon resonance wavelength and the plasmon lifetime on the interparticle distance was reported. This phenomenon was investigated by conventional far-field spectroscopy. Since the physical origin of the observed effects is expected to be connected to the *local* electromagnetic fields acting on the individual nanoparticles, direct measurement of these local field intensities by near-field optical microscopy is a promising task.

In this article we examine the optical near-field zone of regularly arranged gold nanoparticles by means of a photon scanning tunneling microscope[12] (PSTM) operated in constant-height mode. Previous work has established that the PSTM is capable of measuring the near-field intensity distribution around nanoscale metal samples.[10,13–16] We investigate a small regular 2D grating consisting of 3×3 gold particles with the interparticle distance (grating constant) fixed to 1 μm. We chose this small grating for the investigation of the near-field zone of regularly arranged nanoparticles as it constitutes the transition case between the individual particle and the (infinitely) extended grating.

II. EXPERIMENTAL AND THEORETICAL BACKGROUND

Samples consisting of gold particles with a diameter of 100 nm and a height of 40 nm are produced by EBL performed on a modified scanning electron microscope (SEM). As the substrate an indium tin oxide (ITO) doped glass plate is used to provide the weak electric conductivity required for EBL and SEM in order to avoid charging effects. Further details on EBL are provided elsewhere.[7] After fabrication, a standard characterization of the samples is performed. The SEM is used to check overall quality of the samples, and shape and lateral size of the particles, while atomic force microscopy (AFM) allows a cross-check and measurement of the particle height. Optical extinction spectroscopy at normal incidence is accomplished to find the resonance wavelengths of the particle plasmons. As the overall size of

samples produced by EBL is limited to about 100 μm, a spectrometer coupled to a microscope equipped with a low numerical aperture (0.075) objective is used.

To probe the optical near field of the gold nanostructures we applied a PSTM. In this setup a laser source is used to inject light in a glass prism under total internal reflection conditions. A polarizer is placed between the laser and the prism for polarization control. Optical coupling between prism and substrate is provided by immersion oil. Under these conditions, the light distribution above the sample plane corresponds to a evanescent field with its intensity decaying exponentially with distance from the surface. The effective wavelength of the exciting light turns out to be $\lambda_{eff} = \lambda_0 / n \sin\theta_i$, where λ_0 is the light wavelength in vacuum, n is the effective index of refraction of the prism, and θ_i is the angle of incidence. The local probe is a tapered optical fiber fabricated by means of the so-called tube-etching method,[17,18] which yields small taper apexes (diameter smaller than 100 nm) and a very smooth taper surface. The light field close to the sample is scattered by the glass fiber apex and guided through the optical fiber to a photomultiplier detector. The whole scanning and acquisition system is provided by a commercial AFM. PSTM was the instrument of choice since, as previously established, PSTM images acquired with dielectric fiber tips represent to a good approximation maps of the square modulus of the local electric field around a sample.[4,10,19,20] This makes it possible to perform a direct comparison of PSTM images with theoretical simulations, discarding any interaction of the probe tip with the sample. In contrast, recently published results[21] indicate that the metal coating applied to fiber tips to form an aperture in illumination-mode scanning near-field optical microscopy exerts a crucial influence on the image characteristics of particle plasmon fields excited in gold nanoparticles. One technically important point in our experiments is the procedure of approaching the probe to the sample surface. As we found bare dielectric fiber tips (no metal coating applied) to be inevitably damaged by shear-force operation, we use the exponentially decaying intensity of the exciting evanescent light field as the distance dependent quantity to control the approach, similar to a method previously reported.[10,19] We approach the fiber tip to the sample until a strong increase in the detected light signal reveals the evanescent field and thus the immediate vicinity of the sample. Note that at this stage of operation the actual distance between probe and sample is unknown. Once the evanescent field is detected, we start to acquire PSTM images in constant-height mode. This mode is used in order to avoid any topography induced artifacts that might show up when working in constant-distance mode, whatever the feedback system used.[22–25] Between two subsequent images, we move the probe closer to the sample by $\Delta z = 10$ nm. After a final approach step the probe is touching the sample, thereby ending the experiment. The piezoactuator position for the last image is the zero reference for evaluating the distances from the sample surface at which the previous images have been acquired. In particular, the last unperturbed image is acquired at a distance smaller than Δz, which in principle is only limited by the mechanical stability of the PSTM and the noise level of the

electronics. The advantages of our approach procedure are clearly that we prevent the bare fiber tip from being damaged during scanning and that we gain a 3D data set by acquiring PSTM images at different probe-to-sample distances. As a disadvantage we note the absence of topographical information simultaneously acquired with the PSTM images. This we partly compensate by measuring sample topography by AFM before taking PSTM images.

For a comparison of the experimental PSTM images with theory we apply the Green's dyadic technique (GDT), which relies on a real-space discretization of the objects under investigation. This technique constitutes a reliable tool for simulation of the interaction of light with nanoscale objects, dielectric as well as metallic. First, the electric field is determined self-consistently inside the object. Then knowledge of the Green's dyadic associated with a reference system (the sample substrate) allows one to compute the electric field at any observation point. Details of the basics of the GDT are beyond the scope of this paper, and can be found in recently published literature.[26] For the calculations the gold particles are discretized by cubic cells with a side length of 10 nm to give particle dimensions of $100 \times 100 \times 40$ nm^3. The dielectric function of gold is taken from Ref. 26, and the effective dielectric constant of the substrate is set to 2.37, to account for the ITO doping of the glass substrate. The illumination conditions correspond to the experimentally relevant parameters. As we established previously,[4,10,19,20] calculated maps of the square modulus of the electric field in an observation plane parallel to the substrate plane fit well to experimental PSTM images acquired in constant-height mode. However, in the calculations the distance of the observation plane from the substrate has to be considered somewhat larger than the value known from the experimental parameters (around 50 nm above the substrate plane, i.e., about 10 nm above the top of the particles), in order to match to the experimental PSTM images.[4,10] This *effective* observation height, around 140 nm, is due to the finite size of the fiber tip and consequently an integrated signal pickup over a finite fiber tip volume. This finding has been corroborated recently by results reported in Ref. 27. In order to refine the consideration of the finite tip volume in the calculations presented in this work we use an approach different from the concept of an effective observation height. Rather, we calculate the detected intensity at a given lateral position above the sample by averaging the square modulus of the electric field within the volume of a model tip centered above the considered position. The tip volume is modeled as that of a cone truncated to yield a flat face with a diameter of 40 nm facing the sample, while the cone angle is set to 15°. These parameters were derived from a determination of the shape of the fiber tip apex region with high-resolution transmission electron microscopy. The flat face of the truncated cone is positioned at a height above the sample corresponding to the experimental parameter, and the overall height of the tip is fixed to 200 nm. Comparison of calculated and experimental PSTM images allows us to deduce the lateral position of the nanoparticles with respect to the optical features found in the PSTM images. We note that even simultaneously acquired topography data, as provided in a shear-force controlled constant-distance mode using
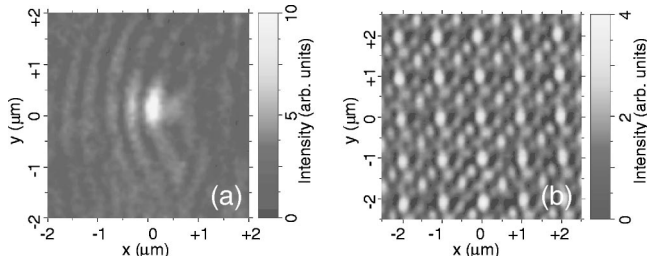
FIG. 1. PSTM images of (a) an isolated gold particle and (b) an ensemble of gold particles arranged in a 2D regular pattern (grating constant $d=1$ μm). In both cases diameter parallel to the substrate and height of the individual particles are 40 and 100 nm, respectively. The exciting light is incident from left to right, $\lambda_0 = 633$ nm, TM polarization, $\theta_i = 43.7°$.

metal coated fiber tips, does not necessarily provide this information with sufficient accuracy in our specific case. This is due to (1) the limited lateral resolution of the topographical images of around 100 nm and (2) a possible lateral shift between topographic and optical features in the corresponding images, due to the spatial separation of the points of shear-force and optical interaction on the fiber tip.[23]

III. RESULTS AND DISCUSSION

We start with the optical response of a resonantly excited single isolated gold nanoparticle similar to the one investigated in previous work.[10] In Fig. 1(a) the light intensity distribution around such a feature as measured by PSTM is shown. As in all the images presented here, the projection of the wave vector of the incoming light on the substrate plane is oriented mainly from left to right, and the distance between tip and sample is less than 10 nm. As already reported in Ref. 10, a rather broad bright spot due to forward scattering, together with a pattern of standing waves due to interference between the incident and backscattered propagating surface waves, is clearly visible. In contrast, a strong confinement of light has been observed above a 1D chain of gold nanoparticles for a particular distance between the particles as reported in Ref. 10. Going one step further in structural complexity, we turn to gold nanoparticles arranged in a large 2D square grating. A PSTM image of such a grating consisting of 200×200 particles with a grating constant fixed to 1 μm is shown in Fig. 1(b). For both the single particle and the particles within the extended grating, height and diameter were set to 40 nm and 100 nm, respectively. The incident light was TM polarized, $\lambda_0 = 633$ nm, and θ_i was set to 43.7°. The PSTM images clearly demonstrate that the light field distribution above the grating cannot be considered simply as the superposition of the light field intensities of isolated particles. Rather, we find particular spatial profiles of the bright spots in the two images and additional maxima and minima in light intensity within the area of the grating, obviously due to interference effects. As already outlined above, this finding led us to study the transition case of a grating consisting of only 3×3 particles. We expect this intermediate case to simplify the interpretation of PSTM images compared to the extended grating. A SEM image of the
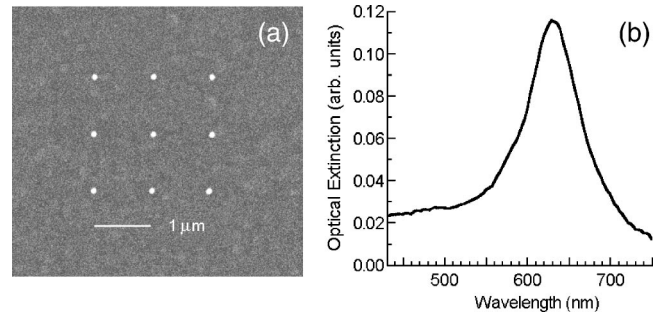

FIG. 2. (a) SEM image of a 3×3 gold particle grating. The diameter of the particles parallel to the substrate is 100 nm and the particle height is 40 nm. The grating constant is 1 μm. (b) Corresponding extinction spectrum showing the plasmon resonance wavelength at 630 nm.

3×3 particle grating is shown in Fig. 2(a). The grating constant of 1 μm was choosen to exclude any grating induced effects[11] in the considered spectral range as discussed briefly in Sec. I. Figure 2(b) displays the extinction spectrum corresponding to a sample containing many 3×3 particle gratings. We find the resonance wavelength of the particle plasmon driven parallel to the substrate plane to be located close to a vacuum wavelength of 633 nm.

We now turn to PSTM images of the 3×3 gold particle grating. Figure 3 displays a PSTM image over 5×5 μm^2 for a laser wavelength $\lambda_0 = 488$ nm, TM polarization, and an incident angle $\theta_i = 43.7°$. As in the case of the isolated particle we find a pattern of standing waves around the particle grating. In front of the grating (left side of the image) the standing wave pattern shows a spatial periodicity of about 240 nm, corresponding closely to half the effective wavelength of the incident light $\lambda_{eff}/2$. This pattern is attributed to interference of the incoming and backscattered surface waves. Standing waves also appear on the sides of the grating (upper and lower sides of the image). Here the fringes of the standing wave pattern are oriented at an angle
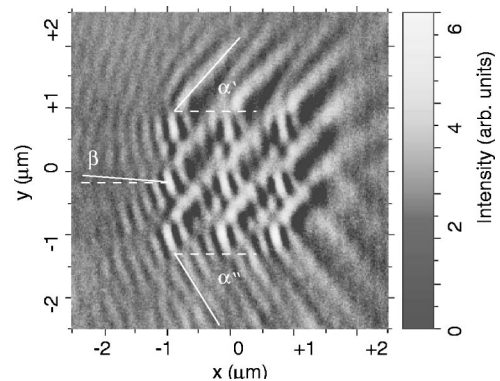

FIG. 3. PSTM image over 5×5 μm^2 of the 3×3 gold particle grating for off-resonant particle plasmon excitation. $\lambda_0 = 488$ nm, TM polarization, $\theta_i = 43.7°$. The angle α formed by the fringes of the standing waves with the horizontal direction is $\alpha' = 48°$ and $\alpha'' = 58°$ on the upper and lower borders of the grating, respectively. Thus, the inclination of the incoming light turns out to be $\beta = 5°$ approximately.
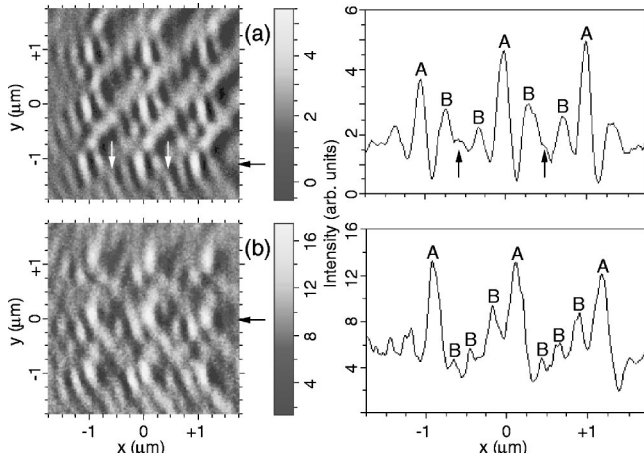
FIG. 4. PSTM images of the 3×3 gold particle grating for off-resonant particle plasmon excitation ($\lambda_0 = 488$ nm, $\theta_i = 43.7°$). (a) TM and (b) TE polarization. The cross sections are taken on horizontal rows in the images, as indicated by the arrows.

α with respect to the horizontal x axis. This is due to interference between the incident wave and the scattered one propagating at an angle 2α with respect to the horizontal x axis. The different spatial periodicity of the interference pattern is in agreement with the geometrical constraint that imposes a correction factor $1/\sin \alpha$. The distance between two adjacent fringes of the interference pattern is 280 nm on the lower and 310 nm on the upper side of the image, corresponding to two different values of α, as shown in Fig. 3. The difference between the two values of α can be attributed to an inclination of the plane of light incidence from the horizontal x axis of $\beta = 5°$. Furthermore, we find maxima and minima in light intensity due to interference within the particle grating.

In Figures 4 and 5 a full set of PSTM images of the 3 $\times 3$ grating is shown, corresponding to particles excited off ($\lambda_0 = 488$ nm) and in ($\lambda_0 = 633$ nm) resonance, respectively. In both cases the dependence of the distribution of
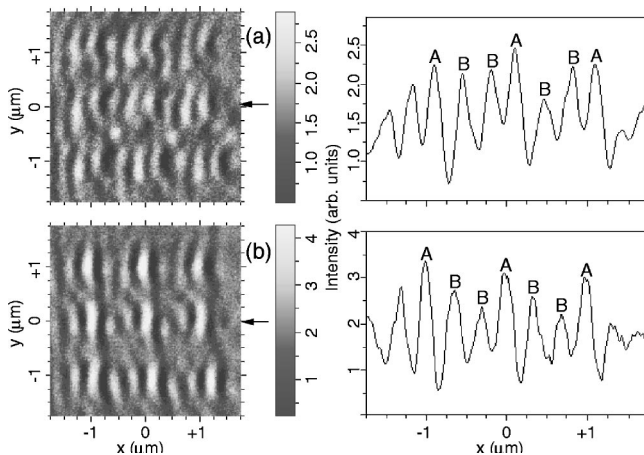

FIG. 5. PSTM images of the 3×3 gold particle grating for resonant particle plasmon excitation ($\lambda_0 = 633$ nm, $\theta_i = 43.7°$). (a) TM and (b) TE polarization. The cross sections are taken on horizontal rows in the images, as indicated by the arrows.

light intensity on the polarization of the incident light is investigated by collecting images in both TM and TE conditions, for an angle of incidence of $\theta_i = 43.7°$. Cross sections taken at horizontal lines in the PSTM images as indicated by the arrows are also displayed.

We first discuss the off-resonant case (Fig. 4). When exciting the sample with TM polarized light [Fig. 4(a)] the PSTM map displays bright spots A appearing with a periodicity corresponding to the grating constant $d = 1$ μm as the most prominent features. Between two consecutive spots A three more bright spots B of lower intensity are found. Due to the above mentioned misalignment one of these maxima (marked by the arrows in the images and the cross section) is only barely visible. Taking the misalignment into account, we conclude that the average relative distance between the spots B is 250 nm. This value corresponds closely to the expected periodicity of interference maxima, i.e., half the effective wavelength of 234 nm. For TE polarization [Fig. 4(b)], we find bright spots A next to a large zone of low intensity that again show a spacing equal to the grating constant $d = 1$ μm. Between two consecutive spots A three intensity maxima B are found, corresponding to the expected periodicity for an interference pattern.

For the resonant case (Fig. 5) a laser wavelength of 633 nm was used to match the particle plasmon resonance. Analogous considerations apply as for the off-resonant case for both TM and TE polarization. Again, we take the most prominent bright feature for TM as well as TE polarization as the reference spots A. The distance between these spots fits with the grating constant of 1 μm. In the resonant case, the number of intermediate features B is different from the off-resonant case, namely, two instead of three. Indeed, this result fits with the exciting wavelength used here, since the expected periodicity of the interference pattern $\lambda_{eff}/2$ is now close to 300 nm. The PSTM images obtained in this experiment suggest a misplacement of the bottom right particle. This was confirmed by imaging the sample topography by AFM.

For validation of our results we now turn to a comparison with numerical simulations based on the GDT. The calculated maps of the electric field intensity for off-resonant particle excitation in TM and TE polarization are displayed in Figures 6(a) and 6(b), respectively. For the case of TM polarization, the calculated map of the electric field intensity is shown in Fig. 6(a), together with a cross section along a horizontal line as indicated in the image by the arrow. As we find from a comparison of the cross section shown in Fig. 6 with Fig. 4, the experimental results are well reproduced by the numerical simulation. In particular, the calculated image confirms the position of the bright spot B barely visible in the experimental image. For TE polarization also [Fig. 6(b)], excellent agreement with the experimental profile is achieved. In particular, the calculation reproduces the intensity of the spots B increasing from left to right. We now compare experiment and simulations to recover the lateral positions of the nanoparticles. In the simulated images, the positions are indicated for one row of particles by the white squares and the black rectangles in the images and the cross sections, respectively. Therefore we find the near-field signature of a
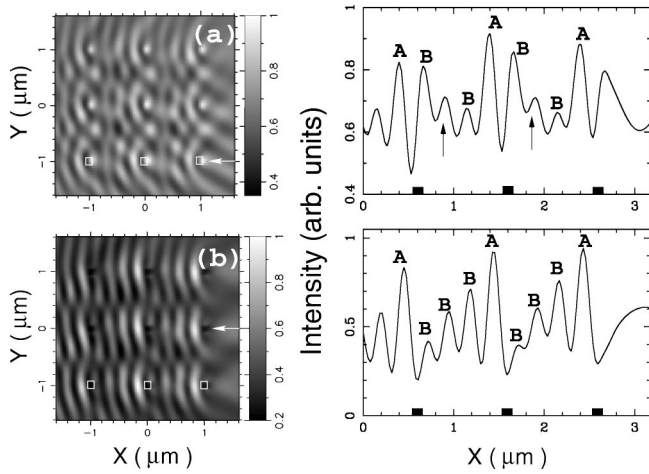
FIG. 6. Calculated maps of the square modulus of the electric field above a 3×3 gold particle grating with a grating constant of 1 μm for the off-resonant case ($\lambda_0=488$ nm, $\theta_i=43.7°$). For the averaging algorithm applied see the text. For compatibility with the experimental images in Fig. 4 the projection of the wave vector of the incoming light on the substrate plane was tilted by $\beta=5°$ (compare Fig. 3. (a) TM and (b) TE polarization. The maximum electric intensity is normalized to 1. The positions of three particles are marked by the white squares (left) and black rectangles (right).

gold nanoparticle to be strongly dependent on the polarization of the incident light, displaying a bright contrast for TM and a dark contrast for TE polarization.

Similar considerations apply in the case of resonantly excited particle plasmons (see Fig. 7). The resemblance of the relative intensities of the individual features found in experiment and calculation is somewhat worse in this case. However, the overall shape of the features as well as the number of interference maxima are well reproduced.
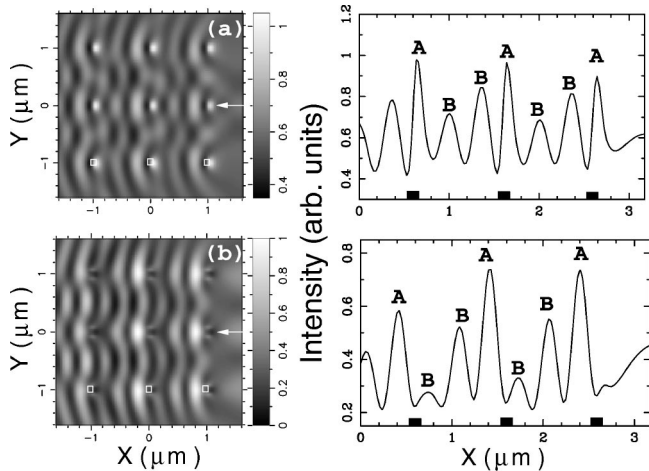

FIG. 7. Calculated maps of the square modulus of the electric field above a 3×3 gold particle grating with a grating constant of 1 μm for the resonant case ($\lambda_0=633$ nm, $\theta_i=43.7°$). For the averaging algorithm applied see the text. (a) TM and (b) TE polarization. The maximum electric intensity is normalized to 1. The positions of three particles are marked by the white squares (left) and black rectangles (right).
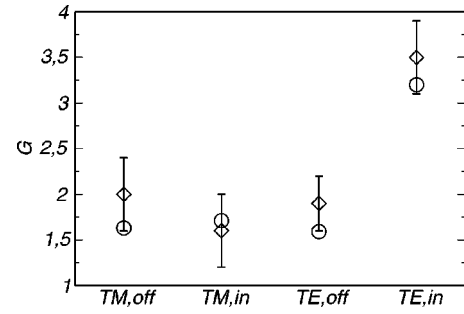

FIG. 8. Measured (diamonds) and calculated (circles) values of the intensity enhancement for the particle plasmon excitation conditions indicated along the abscissa.

Connected to the excitation of particle plasmons, a strong increase of the optical near-field intensity is expected. We estimate the enhancement factor by calculating the ratio between the measured average intensity of the maxima in optical intensity above the grating and the intensity of the driving evanescent field as measured on the flat substrate. The results from the measured PSTM images in Figs. 4 and 5 are marked by the diamonds in Fig. 8. In TE polarization the resonant case provides a clearly larger enhancement ($G_{in,TE}=3.5\pm1.0$) than the off-resonant case ($G_{off,TE}=1.9\pm0.3$), as expected. On the other hand, in TM polarization no enhancement is observed for resonant excitation ($G_{in,\mathrm{TM}}=1.6\pm0.4$) as compared to the off-resonant case ($G_{off,\mathrm{TM}}=2.0\pm0.4$). The maximum enhancement observed fits well with values found from PSTM measurements previously reported.[13,27] However, it is about an order of magnitude smaller than values for particle plasmon induced intensity enhancement known from the literature.[28,29] This effect is again due to the finite detection volume of the fiber tip. Considering an effective observation height of 140 nm, we observe a correspondingly lower plasmon induced intensity enhancement, as the intensity enhancement drops strongly with distance from the particle. Indeed, enhancement values calculated for an effective observation height of 140 nm as marked by the circles in Fig. 8 agree well with the experimental results. The apparent absence of an enhancement in the TM case is simply due to the specific three-dimensional plasmon field profile around the nanoparticle, which leads to almost identical optical signal levels as detected by a dielectric fiber tip in both cases, resonant and off-resonant excitation. Choosing smaller values for the effective observation height in the simulations allows one to calculate the particle plasmon induced intensity enhancement in the immediate vicinity of the nanoparticle. Thereby we find a maximum intensity enhancement factor for a resonant excitation of our particular particle geometry of about 30.

IV. CONCLUSION

We successfully applied a PSTM operated in constant-height mode to probe the near-field optical response of a regular array consisting of 3×3 gold nanoparticles. On one hand, the investigations emphasized the influence of the illumination conditions, such as the polarization, on the apparent

profiles of the features in the near-field images. On the other hand, the properties of the single metal nanoparticles as plasmon resonators were probed when the exciting light is tuned to the proper resonance wavelength. Indeed, under appropriate conditions particle plasmons appeared as a clear increase in the light field enhancement. In the PSTM images of the 3×3 particle grating we found a spatial intensity profile clearly different from that of the single particle. The number of interference maxima within the grating depends on the ratio of the grating constant and the light wavelength. There is obviously no crucial influence of the relative particle position and therefore of the number of nearest neighboring particles (within the array or not) on the spatial intensity profile. The orientation of the fringes of the standing wave pattern outside the grating can be explained by diffraction due to the grating properties of the sample. Our experimental near-field results were supported by calculations based on the GDT. The calculated images reproduced the main features of the PSTM images, i.e., a high intensity spot in TM polarization and a low intensity spot in TE polarization, with the same periodicities as in the experimental images. Moreover, we recovered the measured particle plasmon induced field enhancement in the calculations.

[1] U. Kreibig and M. Vollmer, *Optical Properties of Metal Clusters*, Vol. 25 of *Springer Series in Material Science* (Springer, Berlin, 1995).

[2] C. Bohren and D. Huffman, *Absorption and Scattering of Light by Small Particles* (John Wiley, New York, 1983).

[3] M. Quinten, A. Leitner, J. R. Krenn, and F. R. Aussenegg, Opt. Lett. **76**, 4056 (1998).

[4] J. R. Krenn, J. C. Weeber, A. Dereux, E. Bourillot, J. P. Goudonnet, B. Schider, A. Leitner, F. R. Aussenegg, and C. Girard, Phys. Rev. B **60**, 5029 (1999).

[5] J. C. Weeber, A. Dereux, C. Girard, J. R. Kreen, and J. P. Goudonnet, Phys. Rev. B **60**, 9061 (1999).

[6] H. Ditlbacher, J. R. Krenn, B. Lamprecht, A. Leitner, and F. R. Aussenegg, Opt. Lett. **25**, 563 (2000).

[7] W. Gotschy, K. Vonmetz, A. Leitner, and F. R. Aussenegg, Appl. Phys. B: Lasers Opt. **63**, 381 (1996).

[8] W. Gotschy, K. Vonmetz, A. Leitner, and F. R. Aussenegg, Opt. Lett. **21**, 1099 (1996).

[9] M. Meier, A. Wokaun, and P. F. Liao, J. Opt. Soc. Am. B **2**, 931 (1985).

[10] J. R. Krenn, A. Dereux, J. C. Weeber, E. Bourillot, Y. Lacroute, J. P. Goudonnet, B. Schider, W. Gotschy, A. Leitner, F. R. Ausenegg, and C. Girard, Phys. Rev. Lett. **82**, 2590 (1999).

[11] B. Lamprecht, G. Schider, R. T. Lechner, J. R. Krenn, A. Leitner, F. R. Aussenegg, Phys. Rev. Lett. **84**, 4721 (2000).

[12] R. C. Reddick, R. J. Warmack, and T. L. Ferrell, Phys. Rev. B **39**, 767 (1989).

[13] J. R. Krenn, W. Gotschy, D. Somitsch, A. Leitner, and F. R. Aussenegg, Appl. Phys. A: Mater. Sci. Process. **61**, 541 (1995).

[14] J. R. Krenn, R. Wolf, A. Leitner, and F. R. Aussenegg, Opt. Commun. **137**, 46 (1997).

[15] S. I. Bozhevolnyi and V. Coello, Phys. Rev. B **58**, 10 899 (1998).

[16] S. I. Bozhevolnyi, V. A. Markel, V. Coello, W. Kim, and V. M. Shalaev, Phys. Rev. B **58**, 11 441 (1998).

[17] P. Lambelet, A. Sayah, M. Pfeffer, C. Philipona, and F. Marquis-Weible, Appl. Opt. **37**, 7289 (1998).

[18] R. Stöckle, C. Fokas, V. Deckert, R. Zenobi, B. Sick, B. Hecht, and U. P. Wild, Appl. Phys. Lett. **75**, 160 (1999).

[19] J. C. Weeber, E. Bourillot, A. Dereux, J. P. Goudonnet, Y. Chen, and C. Girard, Phys. Rev. Lett. **77**, 5332 (1996).

[20] A. Dereux, C. Girard, and J. C. Weeber, J. Chem. Phys. **112**, 7775 (2000).

[21] L. J. Richter, C. E. Jordan, R. R. Cavanagh, G. W. Bryant, A. Liu, S. J. Stranick, C. D. Keating, and M. J. Natan, J. Opt. Soc. Am. A **16**, 1936 (1999).

[22] R. Carminati, A. Madrazo, M. Nieto-Vesperinas, and J. J. Greffet, J. Appl. Phys. **82**, 501 (1997).

[23] B. Hecht, H. Bielefeldt, Y. Inouye, D. W. Pohl, and L. Novotny, J. Appl. Phys. **81**, 2492 (1997).

[24] S. I. Bozhevolnyi, J. Opt. Soc. Am. B **14**, 2254 (1997).

[25] R. L. Williamson, L. J. Brereton, M. Antognozzi, and M. J. Miles, Ultramicroscopy **71**, 165 (1998).

[26] C. Girard and A. Dereux, Rep. Prog. Phys. **59**, 657 (1996).

[27] V. A. Markel, V. M. Shalaev, P. Zhang, W. Huynh, L. Tay, T. L. Haslett, and M. Moskovits, Phys. Rev. B **59**, 10 903 (1999).

[28] P. W. Barber, R. K. Chang, and H. Massoud, Phys. Rev. B **27**, 7251 (1983).

[29] B. Lamprecht, J. R. Krenn, A. Leitner, and F. R. Aussenegg, Phys. Rev. Lett. **83**, 4421 (1999).